

## Spin-flip probability in the inelastic scattering of 15–40 MeV protons on light nuclei

R. De Leo, G. D'Erasmus, E. M. Fiore, G. Guarino, and A. Pantaleo

*Istituto di Fisica dell'Università di Bari, Bari, Italy*

*and Istituto Nazionale di Fisica Nucleare, Sezione di Bari, Italy*

S. Micheletti, M. Pignanelli, and L. Serafini

*Istituto di Fisica dell'Università di Milano, Milano, Italy*

*and Istituto Nazionale di Fisica Nucleare, Sezione di Milano, Italy*

(Received 18 May 1981)

Spin-flip probability angular distributions for proton scattering from the  $2_1^+$  level of  $^{24}\text{Mg}$  have been determined between  $25^\circ$  and  $165^\circ$  (in steps of  $10^\circ$ ) at 15 incident energies between 14.5 and 35.5 MeV and, to obtain a more detailed energy dependence at backward angles, spin-flip probabilities have also been measured between  $115^\circ$  and  $165^\circ$  at ten additional energies. In order to extend the study of spin-flip probabilities also to other nuclei and to complement previous angular distributions, further backward angle data have been taken at 13 energies for  $^{32}\text{S}$  and near 40 MeV for  $^{12}\text{C}$  and  $^{28}\text{Si}$ . The experimental results have been compared with coupled-channel calculations based on the rotational model and, for  $^{24}\text{Mg}$ , also with the predictions of microscopic antisymmetrized distorted wave calculations including two-step contributions. The collective analysis proves that spin-flip probabilities are particularly sensitive to the sign of the quadrupole deformation.

NUCLEAR REACTIONS  $^{24}\text{Mg}(p,p'\gamma)$ ,  $E_p = 14.5 - 41.1$  MeV;  $^{32}\text{S}(p,p'\gamma)$ ,  $E_p = 15.5 - 40.9$  MeV;  $^{12}\text{C}(p,p'\gamma)$ ,  $E_p = 41.1$  MeV;  $^{28}\text{Si}(p,p'\gamma)$ ,  $E_p = 35.3, 40.9$  MeV; measured  $\sigma(E_p, \theta_{p'}, \phi_\gamma = 90^\circ)$  for the  $2_1^+$  level; microscopic CC analysis; deduced sign of quadrupole deformation parameters; microscopic ADWBA analysis including two-step GR contributions for  $^{24}\text{Mg}$ .  $^{24}\text{Mg}$  enriched target.  $^{12}\text{C}$ ,  $^{28}\text{Si}$ , and  $^{32}\text{S}$  natural targets.

### I. INTRODUCTION

Macroscopic model predictions for elastic and inelastic scattering of light particles are known to be sensitive to the shape of target nuclei. This is particularly true for analyses based on the coupled-channels (CC) formalism so that these have been used to determine the sign and magnitude of quadrupole deformations from proton,<sup>1,2</sup> deuteron,<sup>3</sup> and  $\alpha$ -particle<sup>4</sup> scattering in  $0_{g.s.}^+ \rightarrow 2_1^+$  transitions in even-even nuclei. The determination of quadrupole deformations allows, moreover, a test of the nuclear model used by a comparison with values derived from electromagnetic transition rates or Coulomb excitation data. While usually only differential cross sections and, less frequently, asymmetry data are considered, another observable,

the spin-flip probability (SFP), determined by measuring the angular correlation function between the scattered nucleon and the ensuing  $\gamma$  ray,<sup>2,5-10</sup> can add useful information. However, the data on SFP's available up to now, due to their scarcity, have not permitted drawing conclusions about nuclear shapes or even the capability of the model in reproducing the experimental results. This failure should also partly be ascribed to the high sensitivity of SFP's to the details of the model<sup>5,10</sup> and to the presence of strong effects due to semidirect contributions. Evidence for two-step processes via a giant resonance (GR) has recently been found.<sup>8,9</sup>

In this paper we present the results of new SFP measurements for transitions to the first  $2^+$  levels of  $^{12}\text{C}$ ,  $^{24}\text{Mg}$ ,  $^{28}\text{Si}$ , and  $^{32}\text{S}$  at incident proton energies between 15 and 41 MeV. These data, together

with other collected in previous experiments<sup>8,9</sup> on  $^{12}\text{C}$  and  $^{28}\text{Si}$ , constitute a set of systematic SFP values spanning different target masses and energies.

The results of the analysis, described in the following sections, provide further evidence for the presence of semidirect contributions over sizeable incident energy regions and support, at the same time, the usefulness of SFP data, in the energy regions where direct contributions are dominant, for obtaining information on the shape and on the collective features of the nuclei.

## II. EXPERIMENTAL METHOD AND RESULTS

The SFP of a nucleon inelastically scattered from an even-even nucleus undergoing a  $0_{g.s.}^+ \rightarrow 2^+ \rightarrow 0_{g.s.}^+$  transition can be determined by measuring the angular correlation function between the inelastically scattered nucleon and the resulting  $\gamma$  ray. When detected in a direction perpendicular to the reaction plane, the latter identifies the deexcitation of the  $M = \pm 1$  substates of the  $2^+$  level. The Bohr<sup>11</sup> theorem shows that these substates are excited only by nucleons flipping their spin in the scattering process. This technique has been used here to measure the SFP.

The experimental setup and the data collection and reduction have been described elsewhere.<sup>8,9</sup> The targets used consisted of an enriched (99.9%)  $^{24}\text{Mg}$  self-supporting foil, 5.73 mg/cm<sup>2</sup> thick, and of a deposit, about 1 mg/cm<sup>2</sup> thick, of natural sulphur on a gold backing. As a check of previous results some additional data have been collected on  $^{12}\text{C}$  and  $^{28}\text{Si}$ . A graphite foil and a natural silicon slice, both about 4 mg/cm<sup>2</sup> thick, have been used for these latter measurements. SFP angular distributions for proton scattering to the  $2^+$  (1.37 MeV) state of  $^{24}\text{Mg}$  have been measured from 25° to 165° in steps of 10°, at 15 energies between 14.5 and 35.5 MeV. These angular distributions are reported in Fig. 1. The experimental errors affecting the SFP, practically due to the statistical indeterminacy only, are larger at high energies due to the increased background  $\gamma$  yield and are indicated with vertical bars.

To study the energy dependence in more detail, further data have been taken, at 10 additional incident energies between 27.5 and 41.1 MeV, in the range between 115° and 165°. The SFP, averaged over six scattering angles (115°, 125°, 135°, 145°, 155°, and 165° laboratory angles), is plotted, as

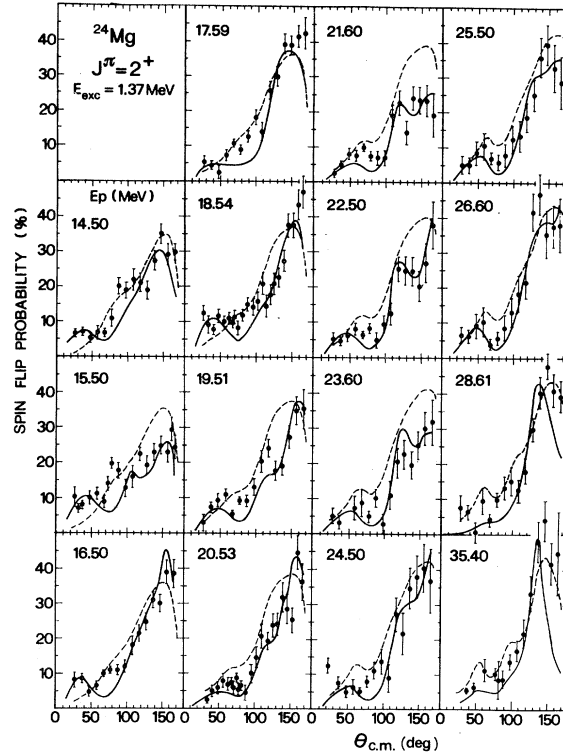


FIG. 1. Angular distributions of the spin-flip probability in proton scattering to the  $2^+$  level of  $^{24}\text{Mg}$ . Dashed curves represent the result of symmetric rotational model CC calculations. Full lines are the result of microscopic ADWBA calculations (see Sec. III B) including two-step GR contributions.

$\langle \text{SFP} \rangle$ , against incident energy in Fig. 2. These six angles allow exploring the angular region containing the backward maximum which is the most prominent structure in the SFP angular distributions. The  $\langle \text{SFP} \rangle$  excitation functions for the other nuclei are also given in Fig. 2. The data for  $^{32}\text{S}$  ( $2^+$  state at 2.33 MeV) have been collected at 14 incident energies between 15.5 and 40.9 MeV. For this nucleus the angular distribution<sup>12</sup> reported in Fig. 7 has also been considered. The excitation of the lowest  $2^+$  state in  $^{12}\text{C}$  ( $2^+$  state at 4.43 MeV) and  $^{28}\text{Si}$  ( $2^+$  state at 1.78 MeV) has been derived from previous studies.<sup>8,9</sup> Additional data have been taken in the present experiment at 41.1 MeV for  $^{12}\text{C}$  and at 35.3 and 40.9 MeV for  $^{28}\text{Si}$ . Most of the above SFP numerical data, together with the cross sections for elastic and inelastic  $2^+$  transitions, measured in the same experiments, have been published elsewhere.<sup>13</sup>

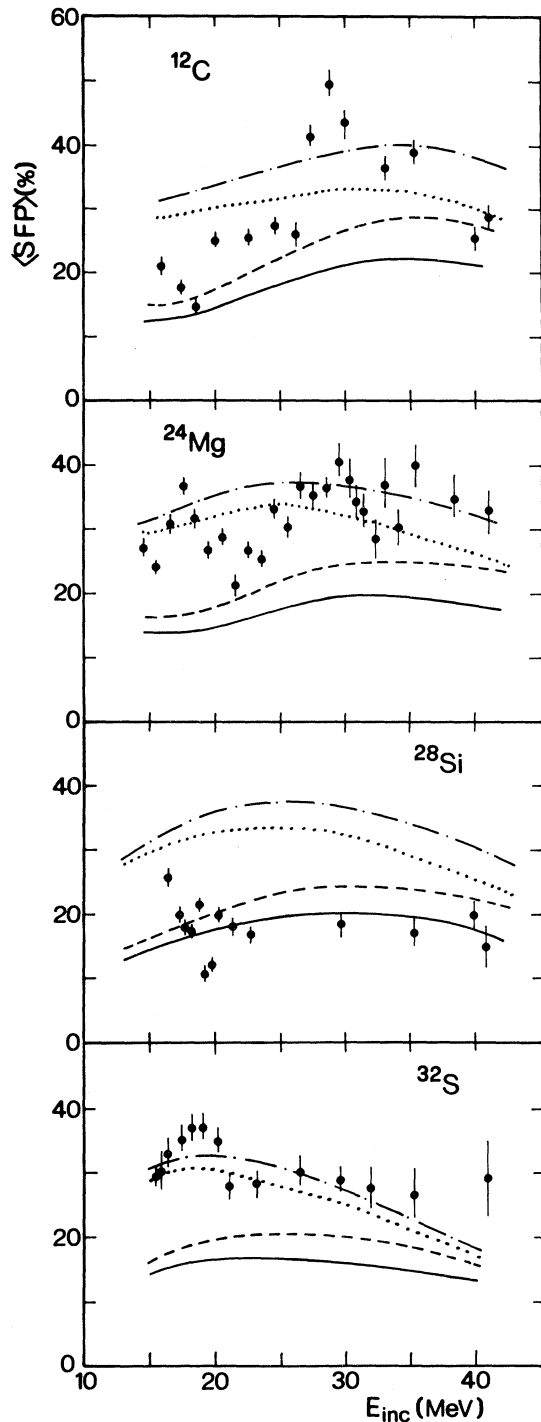


FIG. 2. Spin-flip probabilities to  $2_1^+$  levels averaged over six scattering angles ( $115^\circ - 165^\circ$ ). The curves are the result of symmetric rotational model CC calculations with the OM parameters of Table I and  $\beta_2 > 0$ ,  $\lambda = 1$  (dotted line);  $\beta_2 > 0$ ,  $\lambda = 2$  (dotted and dashed line);  $\beta_2 < 0$ ,  $\lambda = 1$  (full line);  $\beta_2 < 0$ ,  $\lambda = 2$  (dashed line).

### III. DATA ANALYSIS

#### A. Coupled-channels analysis

All the excitation functions of the  $\langle \text{SFP} \rangle$ , given in Fig. 2, show strong energy variations. For  $^{12}\text{C}$  and  $^{24}\text{Mg}$  they are present over a wide energy range extending up to 35–40 MeV, while they are mostly confined below 22 MeV for  $^{28}\text{Si}$  and  $^{32}\text{S}$ . As will be discussed in the next section, these variations can be ascribed to the interfering contributions of higher order processes.

The presence of these processes does not obscure, however, the main features of the direct component, especially at the higher energies. Because of the collective properties of the nuclei considered, which are generally described with the rotational model, this has been evaluated in the framework of CC calculations using the code ECIS.<sup>14</sup> This code permits an automatic search on the values of the parameters, the use of a fully deformed Thomas spin-orbit term<sup>5</sup> and of different values of the deformation for the different terms (real central, imaginary central, and spin-orbit) of the interaction. The parameters of the optical potentials used for the different nuclei are reported in Table I. These have been taken from previous analyses<sup>9,15–17</sup> and have linearly energy dependent depths with fixed geometrical parameters. Some modifications have been required only for the depth of the imaginary terms in order to take into account the channels explicitly considered in the CC calculations. The  $\langle \text{SFP} \rangle$  excitation functions calculated on the basis of the symmetric rotational model and for two values of the ratio ( $\lambda = \beta_2^{\text{so}} / \beta_2^{\text{c}}$ ) of the deformations of the spin orbit and of the central terms are given in Fig. 2. The deformation parameters obtained averaging the best-fit values at the single energies are given in Table II. With  $\lambda = 2$  the deformation  $\beta_2^{\text{c}}$  must be reduced slightly to compensate for the increase in the cross sections due to the larger  $\beta_2^{\text{so}}$  value. The excitation functions corresponding to the choice of the opposite sign for  $\beta_2$  are also given in Fig. 2.

It should be noted that both the sign of  $\beta_2$  and the ratio  $\lambda$  seem to affect the calculated SFP in a very appreciable way. The effect of  $\lambda$  on SFP angular distributions had been previously<sup>5</sup> tested. As seen in Fig. 2 a better fit to the energy dependence of the  $\langle \text{SFP} \rangle$  for  $^{24}\text{Mg}$  and  $^{32}\text{S}$  is obtained with  $\beta_2 > 0$ , in agreement with the prolate shape of these two nuclei. A ratio  $\lambda = 2$  seems also to lead to better agreement at higher energies; an indication of a preference for  $\lambda = 2$  for  $2s-1d$  shell nuclei, far

TABLE I. Energy averaged parameters of CC calculations (potential depths in MeV; lengths in fm).

Nucleus	$V$	$R$	$a$	$W$	$W_D$	$R_W$	$a_W$	$V_{so}$	$R_{so}$	$a_{so}$
$^{12}\text{C}$	$67.4 - 0.4E$	1.064	0.623	0	$4 + 0.1E^a$ $0.11E + 1.99$	1.2	0.600	6.4	1.00	0.600
$^{24}\text{Mg}$	$56.7 - 0.314E$	1.118	0.670	$0^b$ $0.19E - 3$	$3.3 + 0.05E^c$ $7 - 0.12E$	1.336	0.610	5.69	1.00	0.660
$^{28}\text{Si}$	$54.9 - 0.31E$	1.170	0.673	$0^d$ $0.32E - 8$	$6.3^e$ $11.8 - 0.25E$	1.330	0.575	6.0	1.07	0.780
$^{32}\text{S}$	$56 - 0.32E$	1.150	0.718	$0^a$ $0.15E - 3$	$6^a$ $7.6 - 0.08E$	1.252	0.678	5.6	1.01	0.600

<sup>a</sup> $E < 20$  MeV.<sup>b</sup> $E < 16$  MeV.<sup>c</sup> $E < 21.8$  MeV.<sup>d</sup> $E < 25$  MeV.<sup>e</sup> $E < 22$  MeV.

from shell closures, has already been obtained.<sup>18</sup> The  $\langle \text{SFP} \rangle$  values for  $^{28}\text{Si}$  are better fitted with  $\beta_2 < 0$ , in agreement with its oblate shape, and  $\lambda = 1$ . This ratio could be the result of the closure of the  $d_{5/2}$  shell.<sup>18</sup>

As a test of the sensitivity of these calculations to the different collective models and to their parameters, some further comparisons are given in Fig. 3. The quantity is again the  $\langle \text{SFP} \rangle$  at backward angles. A parameter particularly critical in determining the SFP, and not well determined by the cross sections, is the spin-orbit depth  $V_{so}$ . The effect produced, for  $^{24}\text{Mg}$ , varying it by  $\pm 0.5$  MeV with respect to the value of Table I, as shown in the upper part of Fig. 3, is small above about 30 MeV. The larger effect at low energies is reduced when the other optical parameters are readjusted in order to restore the fit to the cross section data.

TABLE II. Quadrupole deformation for the real central terms. The deformation for the imaginary terms has been taken as  $(R_0/R_w)\beta_2^c$  in order to keep constant the scattering length, that for the spin-orbit term as  $(R_0/R_{so})\lambda\beta_2^c$ .

Nucleus	$\beta_2^c$	$\beta_2^c$
	$\lambda = 1$	$\lambda = 2$
$^{12}\text{C}$	-0.60	-0.54
$^{24}\text{Mg}$	0.46	0.428
$^{28}\text{Si}$	-0.32	-0.30
$^{32}\text{S}$	0.30	0.285

In the lower part of Fig. 3 the  $\langle \text{SFP} \rangle$  predicted for  $^{32}\text{S}$  by the vibrational model is compared with that given by the rotational model for the prolate and oblate deformations. It is seen that the first

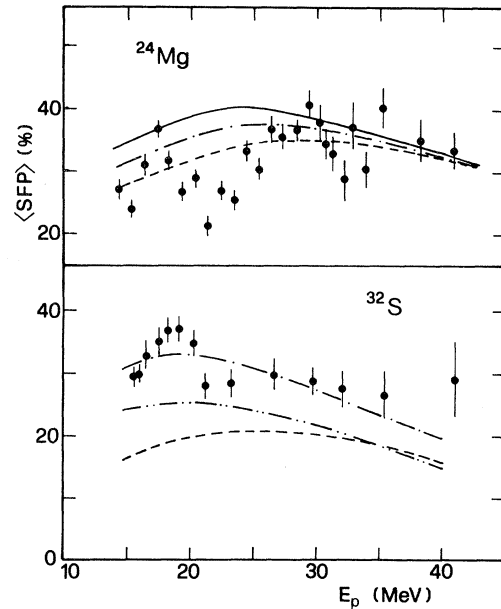


FIG. 3. Predictions for the average spin-flip probability (upper part) for  $V_{so}$  of Table I (dotted and dashed line).  $V_{so} + 0.5$  MeV (full line);  $V_{so} - 0.5$  MeV (dashed line). Shape parameters are  $\beta_2^c = 0.428$  and  $\lambda = 2$ . Predictions (lower part) of CC calculations with  $\lambda = 2$  for different models; rotational model and  $\beta_2 > 0$  (dotted and dashed line); rotational model and  $\beta_2 < 0$  (dashed and dashed line); vibrational model (two dots and dashed line).

model, also suggested (see literature cited in Ref. 16) for the description of  $^{32}\text{S}$ , would require even larger values of  $\lambda$ . From the comparisons in Fig. 3 it is clear that the unavoidable ambiguities in the optical parameters cannot obscure the larger dependence of the  $\langle\text{SFP}\rangle$  on the collective parameters and on the various models.

It is worthwhile to note that, for all the nuclei, the rotational model with prolate deformation ( $\beta_2 > 0$ ) gives, over the all angular range, SFP's which are larger than those obtained with oblate deformation.

The dependence of the  $\langle\text{SFP}\rangle$  on the value of  $\beta_2$  for the two kinds of deformation is shown in Fig. 4. The calculations have been performed for a hypothetical nucleus with the optical model parameters of  $^{24}\text{Mg}$  and  $\lambda=2$ . Surface imaginary depths have been varied in order to maintain approximately constant the value of the reaction cross section. The splitting seen in Fig. 4 is due to the "reorientation term," present only in the rotational model, which couples the level to itself producing a constructive or destructive interference to the SFP, depending on whether  $\beta_2$  is positive or negative. The  $\beta_2$  dependence given by the second order vibrational model is also shown for comparison. It is not dependent on the sign of  $\beta_2$  and gives results which are practically coincident with those of the DWBA.

This large difference between the values of the SFP calculated for prolate and oblate deformations seems to persist, even if of smaller size, also when all the optical model parameters are readjusted in a fit with the "wrong" sign of  $\beta_2$ . This has been confirmed for  $^{28}\text{Si}$  at 30 MeV in best fit tests of all the data available, including the asymmetry<sup>19</sup> for the transitions to the  $2_1^+$  and  $4_1^+$  levels, which gave  $\langle\text{SFP}\rangle$  of 28 and 17%, respectively, for  $\beta_2 > 0$  and  $\beta_2 < 0$ .

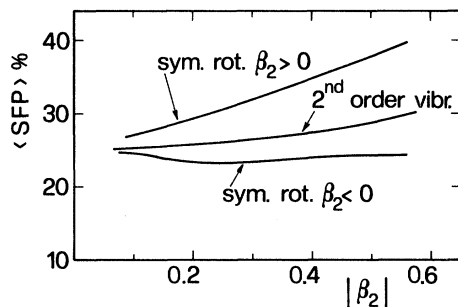


FIG. 4. Dependence of the average spin-flip probability in  $|\beta_2|$ .

A sizeable increment of the  $\langle\text{SFP}\rangle$  is obtained for all the nuclei by increasing  $\lambda$  from 1 to 2 (see Fig. 2). This change generally gives SFP angular distributions with more evident oscillations at forward angles.

The fits to the angular distributions of the SFP confirm the values for the  $\beta$  and  $\gamma$  parameters obtained from the analysis of the  $\langle\text{SFP}\rangle$  excitation functions. The calculated angular distributions for the SFP in  $^{24}\text{Mg}$  obtained with the parameters of Table I and for prolate and oblate deformations and  $\lambda=1,2$  are given in Fig. 5. At 21.6 MeV higher order effects contribute strongly, lowering the SFP at backward angles and causing an apparent better fit with  $\beta_2 > 0$  and  $\lambda=2$ . At still lower energies these effects decrease and at 14.5 MeV a better agreement is again obtained with the values of the parameters deduced from the excitation function and the angular distribution at 35.4 MeV. The CC predictions with  $\beta > 0$  and  $\lambda=2$  are given in Fig. 1 for all the measured energies.

Since  $^{24}\text{Mg}$  is known to be best described as prolate triaxial rotor, the SFP angular distribution at 35.4 MeV has been refitted in a more detailed analysis on the basis of the asymmetric rotational model by readjusting both the depth of the optical potential terms and the shape parameters. Cross sections<sup>13</sup> to the  $0^+, 2^+$ , and  $4^+$  states of the ground state band and to the  $2^+$  state of the  $K=2$   $\gamma$ -vibrational band have been included in the analysis. With  $\lambda=1$  a value of  $\beta_2=0.5$ , larger than the mean value of Table II, is obtained. According to the method of Clement *et al.*,<sup>3</sup> it corresponds to a  $B(E2, 2_1^+ \rightarrow 0_1^+)$  of 18.6 Weisskopf single-particle units obtained using an equivalent charge radius  $R_{oc}=3.808$  fm. This value is in good agreement with that of  $20.5 \pm 0.6$  derived from lifetime measurements.<sup>20</sup> The difference between this value of  $\beta_2$  and the one reported in Table II is due to the inclusion in the CC analysis of the  $4_1^+$  level and not to the use of the asymmetric rotor model. The increase of  $\lambda$  to 1.8, as seen in Fig. 6, improves both the  $2^+$  cross section and the SFP predictions in agreement with the excitation function results. The value of  $\beta_2$  is slightly reduced to 0.47. The hexadecapole deformation  $\beta_4$  is subject to rather large uncertainties; the values obtained for  $\beta_4=-0.55$  and for the asymmetry parameter  $\gamma=20^\circ$  agree, within the error, with those derived in previous proton and  $\alpha$ -particle scattering experiments,<sup>21,22</sup> and are scarcely influenced by the  $\gamma$  value.

A still lower value of the  $\chi^2$  for the SFP is ob-

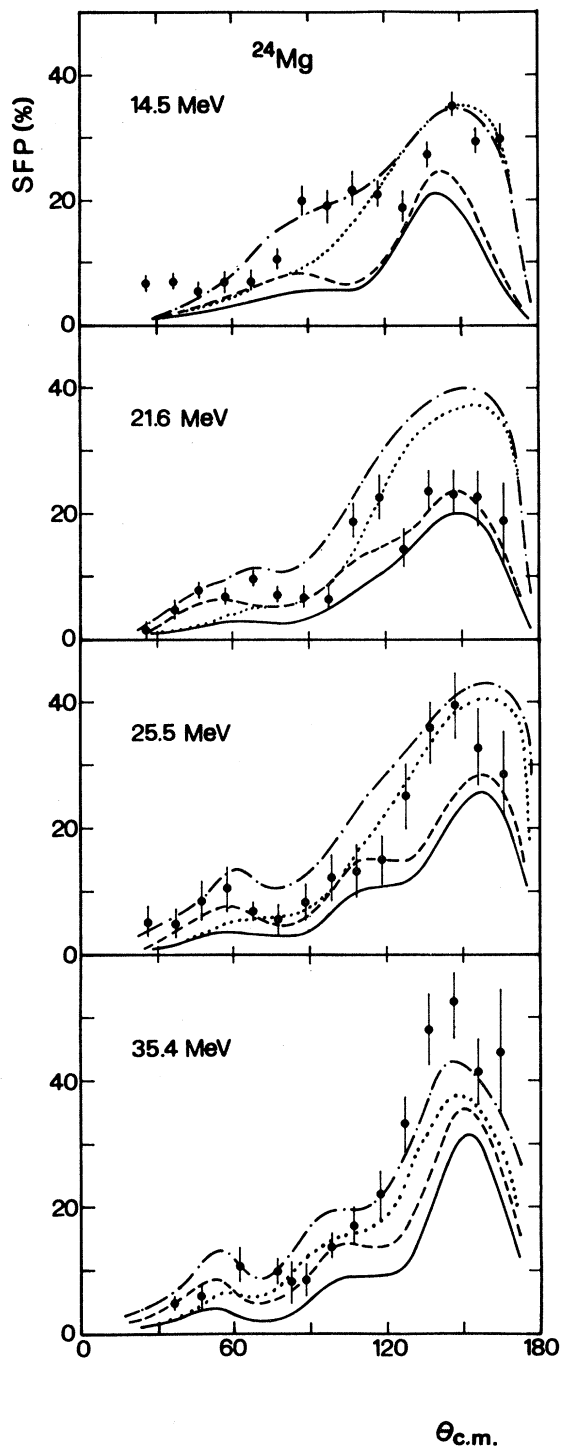


FIG. 5. Rotational model CC predictions for spin-flip probabilities compared with experimental angular distributions for  $^{24}\text{Mg}$  at various energies. The curves are drawn with the same conventions as in Fig. 2.

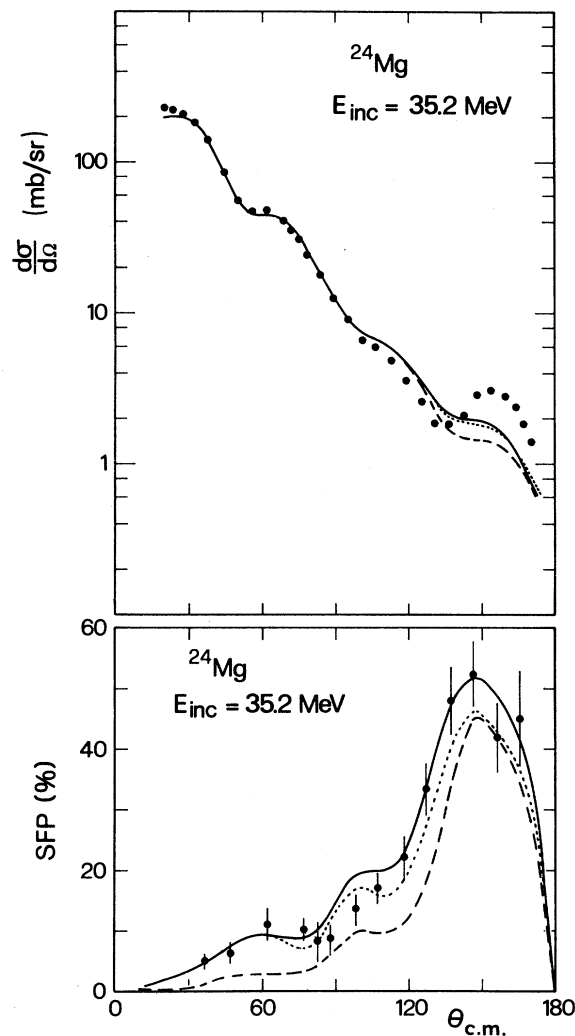


FIG. 6. Experimental cross section and spin-flip probability for the transition to the  $2_1^+$  level of  $^{24}\text{Mg}$  at 35.2 MeV compared with CC best fitted calculations based on the asymmetric rotational model and  $\lambda=1$  (dashed line);  $\lambda=1.8$  (dotted line);  $\lambda=1.8$  and  $\langle 2_1^+ || Q^m || 2_1^+ \rangle$  increased by a factor 1.8 (see Sec. III A) (full line).

tained leaving the quadrupole mass transition amplitude  $\langle 2_1^+ || Q^M || 2_1^+ \rangle$ , corresponding to the static quadrupole moment  $Q_{2_1}$ , free to vary and therefore to change the effect of the “reorientation term.” The best fit value gives, again according to Ref. 3,  $eQ_{2_1} = -26.6$  ( $e \text{ fm}^2$ ), in agreement with those ranging from  $-24$  to  $-27$  ( $e \text{ fm}^2$ ) derived from Coulomb reorientation measurements.<sup>3</sup> The value given by the rotational model with  $\beta_2=0.5$  is  $-17.7$  ( $e \text{ fm}^2$ ).

The SFP angular distributions obtained with the parameters of Table I for  $^{12}\text{C}$ ,  $^{28}\text{Si}$ , and  $^{32}\text{S}$  are given in Fig. 7 for only one value of the incident energy. They generally confirm also for these nuclei the indications obtained from the excitation functions. The indications for  $^{12}\text{C}$  are less straightforward since the energy variations seem to extend to nearly all the energy interval investigated. On the basis of the excitation function (Fig. 2) negative values of  $\beta_2$  seem to be favored at lower energies, while practically equivalent agreement is obtained with  $\beta_2 < 0$  and  $\lambda=2$  or  $\beta_2 < 0$  and  $\lambda=1$  around 40 MeV. However, at high incident energies the SFP at forward and intermediate angles (Fig. 7) is in better agreement with the  $\beta_2 < 0$  and  $\lambda=1$  curve.

In the energy interval of the present analysis, as can be seen from Figs. 6, 8, and 9, calculated cross sections practically do not depend on the value of

$\lambda$ . The sign of  $\beta_2$  affects only slightly the absolute value of the cross sections, so that deformations differing by 10% are required, but leaves practically unaltered the shape of the angular distributions. Asymmetries are instead affected to a substantial degree by the same parameters but not in a way as simple as SFP's (see Figs. 8 and 9). They change differently in different angular ranges and for different nuclei so that the effect of changing the sign of  $\beta_2$  is more easily masked<sup>2</sup> by the ambiguities in the optical-model parameters.

It seems possible to conclude that CC analyses, in spite of the presence of higher order effects at lower energies, describe reasonably well the body of data with physically acceptable optical and collective parameters and are able to distinguish between prolate and oblate deformations.

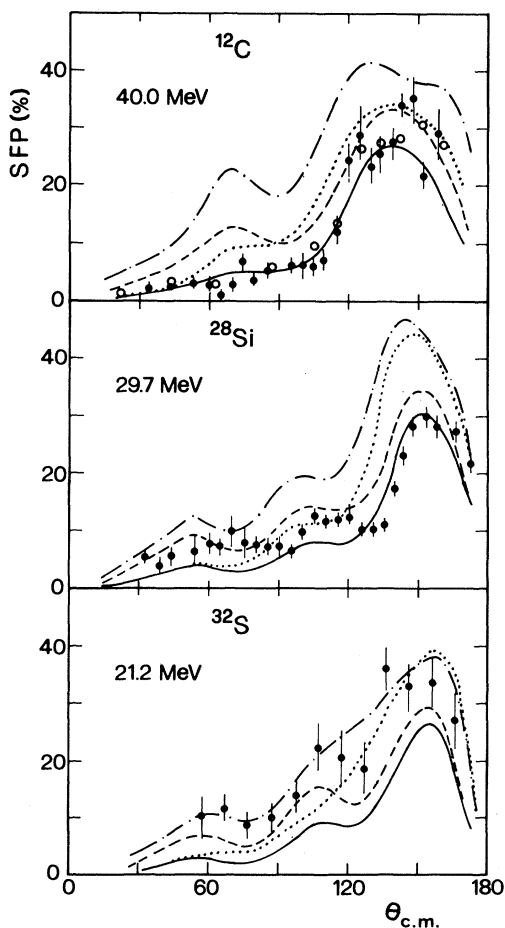


FIG. 7. Comparison of CC predictions with experimental spin-flip probability angular distributions. The curves are drawn with the same convention of Fig. 2.

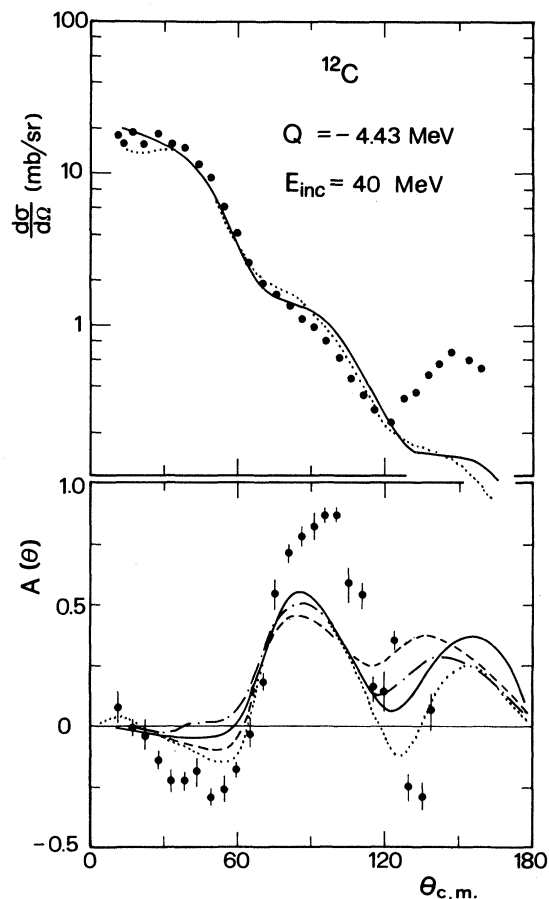


FIG. 8. Experimental differential cross section, and analyzing power for the transition to the  $2^+_1$  level of  $^{12}\text{C}$  compared with CC predictions. The curves are drawn with the same conventions as in Fig. 2. Curves with  $\lambda=2$  for the cross sections practically coincide with those for  $\lambda=1$ .

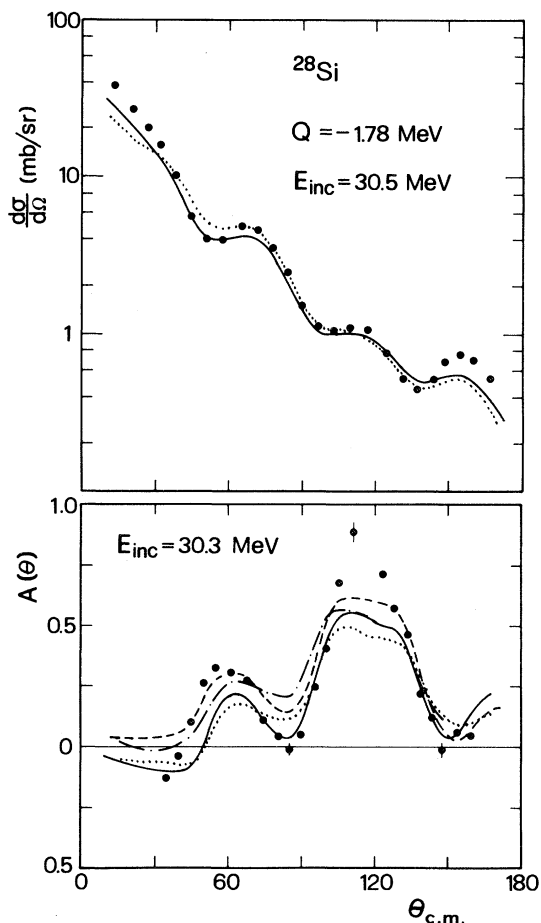


FIG. 9. Experimental differential cross section and analyzing power for the transition to the  $2_1^+$  level of  $^{28}\text{Si}$  compared with CC predictions. The curves are drawn with the same conventions as in Fig. 2.

The effect of the sign of the quadrupole deformation on SFP values for transitions in higher mass nuclei has been calculated for the  $^{58}\text{Ni}$  data of Ref. 6 and the  $^{114}\text{Cd}$  data of Schneider *et al.*<sup>2</sup> The CC curves calculated for the SFP in the transition to the  $2_1^+$  level of  $^{58}\text{Ni}$  at 20 MeV for the rotational model with both signs of  $\beta$  and for the vibrational model are given in the upper part of Fig. 10. The optical potentials and the ratio  $\lambda=2$  of the analysis of Ref. 6 have been used. It is seen that the calculations confirm the vibrational nature of this nucleus. The SFP angular distributions for  $^{114}\text{Cd}$  for different models and deformations have been calculated using the parameter sets given in Table 1 of Ref. 2 (first three lines) and obtained in CC best fit analyses. The author's<sup>2</sup> conclusion that oblate deformation should be ruled out is clearly confirmed.

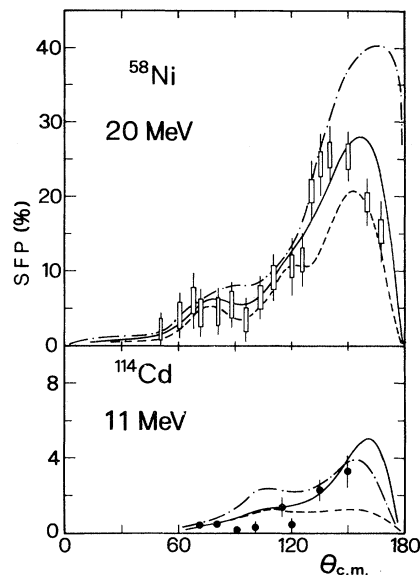


FIG. 10. Experimental spin-flip probabilities to  $2_1^+$  levels from Kolasinsky *et al.* (Ref. 6) and Schneider *et al.* (Ref. 2) in comparison with CC predictions for different models: vibrational (full line), rotational with  $\beta_2 > 0$  (dashed and dotted line), rotational model with  $\beta_2 < 0$  (dashed line). For  $^{58}\text{Ni}$  a ratio  $\lambda=2$  and for  $^{114}\text{Cd}$   $\lambda=1$  have been taken.

### B. Higher order processes

As already noted in Sec. III A, all the  $\langle \text{SFP} \rangle$  excitation functions show strong variations with incident energy over a large part of the energy range. These deviations from the characteristic direct-reaction behavior cannot be due to compound nucleus contributions which are negligible<sup>9</sup> for the transitions considered here, even at low incident energies. As an aid in recognizing the origin of the higher order processes involved, it can be interesting to compare this energy dependence with that of the cross sections for transitions to the lowest unnatural parity states, which are  $J^\pi=3^+$  states, except that of  $^{12}\text{C}$ , which is a  $J^\pi=1^+$  state. In these transitions, in fact, angular momentum and parity conservation rules require a spin flip ( $\Delta S=1$ ) of the proton. Moreover, as the amplitude for the direct processes is strongly reduced by the absence of the  $\Delta S=0$  component, higher order processes are expected to be relatively large. For  $^{12}\text{C}$  and  $^{28}\text{Si}$  it has been already pointed out<sup>8,9</sup> that the energy dependence of the SFP and that of the cross sections of the unnatural parity state are related, in the sense that both can be reproduced by a calcula-

tion in which the antisymmetrized distorted wave Born approximation (ADWBA) amplitude is supplemented by the same resonant contributions. These, in the reaction model given by von Geramb *et al.*,<sup>23,24</sup> are interpreted as due to two-step processes via GR states. Since a detailed description of these calculations has been given by the authors,<sup>23,24</sup> only the main features are reported here. The transition amplitude is given as a coherent sum of single particle amplitudes weighted through a spectroscopic factor specified by the nuclear structure of the levels involved. It contains both "valence" and "core polarization" parts and the respective exchange contributions. The valence terms are calculated using an interaction derived from an effective nucleon-nucleon potential; a deformed collective potential has been used for the calculation of the core polarization terms. It is the exchange core polarization term that formally describes a two-step process via intermediate resonant states. Both  $E1$ ,  $E2$ , and  $E3$  resonances can be included. The complex coupling constants representing the respective strength distributions are derived from the analysis; the inverse procedure, i.e., the use of experimentally determined multipole strengths distributions in the inelastic scattering calculations, generally is not possible because of lack of the phases of the relevant two-step amplitudes.

The above ADWBA analysis, including the two-step contributions, has already been performed<sup>17</sup> for the  $3^+$  (5.2 MeV) state in  $^{24}\text{Mg}$  and has been repeated here for the  $2^+$  state using the same OM parameters and the spectroscopic amplitudes obtained by Wildenthal,<sup>25</sup> and taking into account the present SFP data. The calculations have been performed readjusting the  $E1$ ,  $E2$ , and  $E3$  strengths. Typical results for the SFP's are shown in Fig. 11 for two incident energies. At 23.6 MeV, the  $\chi^2$  procedure used in fitting the  $2^+$  data is dominated by the SFP's. In fact, the SFP predictions without the inclusion of the two-step contributions clearly overestimate the data. This disagreement is not removed by the inclusion, according to the prescription of Satchler,<sup>26</sup> of an imaginary coupling potential in the valence terms. The two-step contributions required are relatively large, particularly for the  $E2$ , and their inclusion leads to a significantly improved fit which is more satisfactory than that given by CC calculations. At the lower energy, 16.5 MeV, the SFP prediction without the inclusion of the two-step contributions is less unsatisfactory and smaller GR contributions

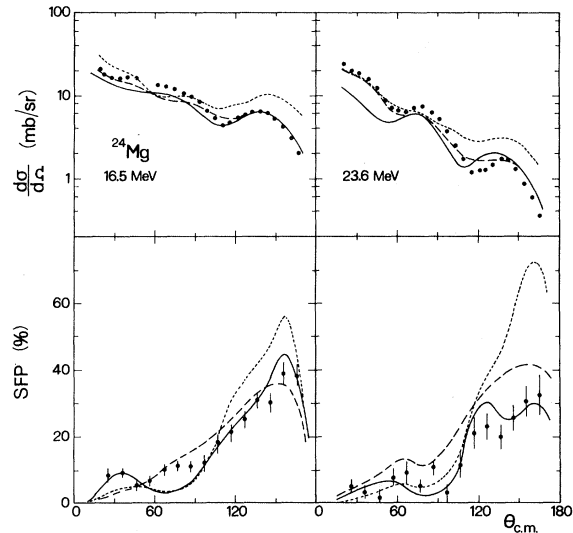


FIG. 11. Effect of the inclusion of the exchange core polarization term of the amplitude in ADWBA calculations: complete calculations (full line), valence and direct core polarization only (dotted lines). The dashed lines represent the results of macroscopic CC calculations as in Fig. 1.

are needed; in this case the final fit is of the same quality of that produced by the CC calculations. The inclusion of the resonant contributions generally improves the fits to the differential cross section at backward angles with some worsening at forward angles where the fitting is dominated by the SFP's. The average quality of the fits remains, however, substantially unvaried and lower than that given by CC calculations.

The results obtained at all the energies for the SFP angular distributions are given in Fig. 1 as continuous lines. The improvement, with respect to CC calculations, is particularly evident in the region around 24 MeV where the  $\langle \text{SFP} \rangle$  oscillates strongly with the energy and the strengths obtained for the various resonances, as given by the amplitude of the coupling constants shown in Fig. 12, are relatively large. It should be stressed that, owing to the fitting procedure used, the trend of these strengths is mainly determined by the energy dependence of the SFP data. The strengths obtained from electroexcitation<sup>27</sup> are also displayed for comparison. An overall agreement is obtained and, in particular, the well known fragmentation<sup>27,28</sup> of the GR in  $^{24}\text{Mg}$  is approximately reproduced. This agreement, together with the fact that the variations of the SFP for the higher mass nuclei  $^{28}\text{Si}$  and  $^{32}\text{S}$  are confined to energies lower than

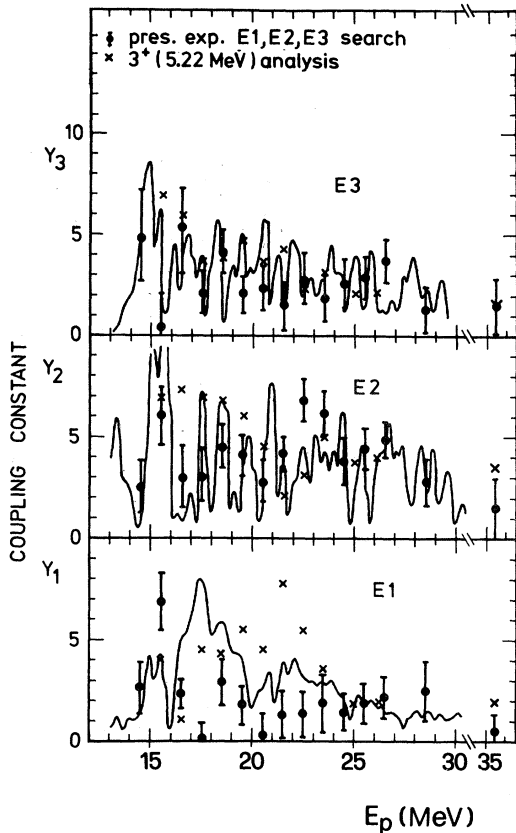


FIG. 12. Energy dependence of the amplitude of the GR coupling constants for  $E1 + E2 + E3$  (full points) determined by fitting the data of Fig. 1. Crosses have been taken from Ref. 17. The lines represent the distribution of GR strength from electroexcitation (Ref. 27); the normalization is the same for the three multiplicities.

22 MeV, again the agreement with the experimental GR strength distributions,<sup>28,29</sup> supports the validity of the hypothesis of the importance of two-step contributions in the prediction of SFP's.

#### IV. CONCLUSIONS

The spin-flip probability (SFP) in proton scattering to  $2^+_1$  levels of light nuclei in the 15–45 MeV incident energy range cannot be interpreted as only a pure one-step direct reaction mechanism. Contributions from two-step processes via giant resonance states are, in fact, present over energy ranges characteristic of each nucleus as evidenced by the energy dependence of the integral of the SFP over the pronounced backward maximum. In spite of these contributions it is nevertheless possible to compare usefully the SFP data with direct reaction model predictions and to discriminate between different macroscopic models. For the nuclei here considered, which are known to be permanently deformed, a simple DWBA calculation is not appropriate and CC calculations, with collective couplings derived from the rotational model, are needed. These analyses prove that SFP's are particularly sensitive to the sign of the quadrupole deformation and can therefore be used to distinguish between prolate and oblate deformations. The SFP's are also sensitive to the relative value of the spin-orbit deformation and to the static quadrupole moment  $Q_{2+}$  for the  $2^+_1$  state.

The authors acknowledge the technical support of Mr. P. Tempesta and of the Milan cyclotron staff.

<sup>1</sup>P. W. F. Alons, H. P. Block, and J. F. A. van Hienen, *Phys. Lett.* **83B**, 34 (1979).

<sup>2</sup>S. Schneider, W. Eyrieh, A. Hofmann, U. Sheib, and F. Vogler, *Phys. Rev. C* **20**, 71 (1979).

<sup>3</sup>H. Clement, R. Frick, G. Graw, F. Merz, P. Scheinenz, N. Seichert, and Sun Tsu Hsun, *Phys. Rev. Lett.* **45**, 599 (1980); K. Hatanaka, M. Nakamura, K. Imai, T. Noro, H. Shimuzu, H. Sakamoto, J. Shirai, T. Matsusue, and K. Nisimura, *ibid.* **46**, 15 (1981).

<sup>4</sup>H. Rebel, *Nucl. Phys.* **A180**, 332 (1972); H. Rebel, G. Hauser, G. W. Schweimer, and G. Nowicki, *ibid.* **A218**, 13 (1974).

<sup>5</sup>H. Sherif and J. S. Blair, *Phys. Lett.* **26B**, 489 (1968);

H. Sherif, *Nucl. Phys.* **A131**, 532 (1969).

<sup>6</sup>W. A. Kolasinski, J. Eenmaa, F. H. Schmidt, H. Sherif, and J. R. Tesmer, *Phys. Rev.* **180**, 1006 (1969); J. J. Kolata and A. Galonsky, *ibid.* **182**, 1073 (1969); D. L. Hendrie, G. Glashauser, J. M. Moss, and J. Thirion, *ibid.* **186**, 1188 (1969); M. A. D. Wilson and L. Schecter, *Phys. Rev. C* **4**, 1103 (1971); R. H. Howell and A. I. Galonsky, *ibid.* **5**, 561 (1972).

<sup>7</sup>R. O. Ginaven, E. E. Gross, J. J. Malanify, and A. Zucker, *Phys. Rev. Lett.* **22**, 552 (1968).

<sup>8</sup>R. De Leo, G. D'Erasmus, F. Ferrero, A. Pantaleo, and M. Pignanelli, *Nucl. Phys.* **A254**, 156 (1975).

<sup>9</sup>R. De Leo, G. D'Erasmus, A. Pantaleo, G. Pasquariello,

- G Viesti, M. Pignanelli, and H. V. Geramb, *Phys. Rev. C* **19**, 646 (1979).
- <sup>10</sup>F. Fujisawa, M. Nakamura, M. Yasue, N. Veda, T. Hasegawa, K. Hatanaka, T. Tanaka, M. Sekiguchi, T. Weda, Y. Taba, F. Soga, and H. Kamitsubo, *Polarization Phenomena in Nuclear Physics—1980*, Fifth International Symposium on Polarization Phenomena in Nuclear Physics, Santa Fe, 1980, edited by G. G. Ohlesen, R. E. Brown, Nelson Jarmie, W. W. McNaughton, and G. M. Hale (AIP, New York, 1981).
- <sup>11</sup>A. Bohr, *Nucl. Phys.* **10**, 486 (1959).
- <sup>12</sup>R. De Leo, G. D'Erasmus, E. M. Fiore, and A. Pantaleo, *Lett. Nuovo Cimento* **28**, 161 (1980).
- <sup>13</sup>R. De Leo, G. D'Erasmus, E. M. Fiore, S. Micheletti, A. Pantaleo, and M. Pignanelli, *Istituto Nazionale di Fisica Nucleare Report INFN/BE-80/3*, 1980.
- <sup>14</sup>J. Raynal, computer code ECIS, CEN Saclay, 1979 (unpublished).
- <sup>15</sup>E. Fabrici, S. Micheletti, M. Pignanelli, F. G. Resmini, R. De Leo, G. D'Erasmus, A. Pantaleo, J. L. Escudicé, and A. Tarrats, *Phys. Rev. C* **21**, 830 (1980).
- <sup>16</sup>R. De Leo, G. D'Erasmus, E. M. Fiore, G. Guarino, A. Pantaleo, and S. Micheletti, *Nuovo Cimento* **59A**, 101 (1980).
- <sup>17</sup>R. De Leo, G. D'Erasmus, E. M. Fiore, A. Pantaleo, M. Pignanelli, and H. V. Geramb, *Phys. Rev. C* **20**, 13 (1979).
- <sup>18</sup>J. Raynal, CEN Saclay Report D. Ph/t n° 71/1, 1971.
- <sup>19</sup>R. De Swiniarski, F. G. Resmini, D. L. Hendrie, and A. D. Bacher, *Nucl. Phys.* **A261**, 111 (1976).
- <sup>20</sup>D. Brandford, A. C. McGough, and I. F. Wright, *Nucl. Phys.* **A241**, 349 (1975).
- <sup>21</sup>R. De Leo, G. D'Erasmus, A. Pantaleo, M. N. Harakeh, S. Micheletti, M. Pignanelli, *Phys. Rev. C* **23**, 1355 (1981).
- <sup>22</sup>K. Van der Borg, M. N. Harakeh, and B. S. Nilsson, *Nucl. Phys.* **A325**, 31 (1979).
- <sup>23</sup>H. V. Geramb, R. Sprickmann, and G. L. Strobel, *Nucl. Phys.* **A199**, 545 (1973); H. V. Geramb, K. Amos, R. Sprickmann, K. T. Knöpfle, M. Rogge, D. Ingham, and C. Mayer-Böricke, *Phys. Rev. C* **12**, 1697 (1975).
- <sup>24</sup>K. Amos and R. Smith, *Nucl. Phys.* **A226**, 519 (1974).
- <sup>25</sup>B. H. Wildenthal, *Elementary Modes of Excitation in Nuclei*, edited by R. Broglia and A. Bohr (North-Holland, Amsterdam, 1977); B. H. Wildenthal, private communication.
- <sup>26</sup>G. R. Sathchler, *Phys. Lett.* **35B**, 279 (1971).
- <sup>27</sup>K. Itoch, S. Ohsawa, Y. Torizuka, T. Saito, and T. Teresawa, *Phys. Rev. C* **23**, 945 (1981).
- <sup>28</sup>F. E. Bertrand, K. van der Borg, A. G. Drentje, M. N. Harakeh, J. van der Plicht, and A. van der Woude, *Phys. Rev. Lett.* **40**, 635 (1978); T. S. Bauer, R. Beurtey, A. Boudard, G. Bruge, H. Katz, P. Couvert, J. L. Escudicé, J. M. Fontaine, M. Garçon, J. L. Lugol, M. Matoba, S. Platchkov, M. Rouger, and Y. Terrien, *Phys. Rev. C* **19**, 1438 (1979).
- <sup>29</sup>K. van der Borg, M. N. Harakeh, S. Y. van der Werf, A. van der Woude, and F. E. Bertrand, *Phys. Lett.* **67B**, 405 (1977).
- <sup>30</sup>D. H. Youngblood, J. M. Moss, C. M. Rozsa, J. D. Bronson, A. D. Bacher, and D. R. Brown, *Phys. Rev. C* **13**, 994 (1976).